Acta Materialia 159 (2018) 384–394

Contents lists available at ScienceDirect

Acta Materialia

journal homepage: www.elsevier.com/locate/actamat

Full length article

Direct volumetric measurement of crystallographic texture using acoustic waves

Bo Lan [a, *], T. Ben Britton [b], Tea-Sung Jun [b, 1], Weimin Gan [c], Michael Hofmann [d], Fionn P.E. Dunne [b], Michael J.S. Lowe [a]

[a] Department of Mechanical Engineering, Imperial College London, Exhibition Road, London, SW7 2BX, UK
[b] Department of Materials, Imperial College London, Prince Consort Road, London, SW7 2AZ, UK
[c] German Engineering Materials Science Centre at MLZ, Helmholtz-Centre Geesthacht, Lichtenbergstr. 1, 85748, Garching, Germany
[d] Heinz Maier-Leibnitz Zentrum (MLZ), Technische Universität München, Lichtenbergstr. 1, D-85747, Garching, Germany

ARTICLE INFO

Article history:
Received 10 July 2018
Received in revised form
20 August 2018
Accepted 21 August 2018
Available online 25 August 2018

Keywords:
Crytallographic texture
Volumetric measurement
Ultrasound
Non-destructive evaluation

ABSTRACT

Crystallographic texture in polycrystalline materials is often developed as preferred orientation distribution of grains during thermo-mechanical processes. Texture dominates many macroscopic physical properties and reflects the histories of structural evolution, hence its measurement and control are vital for performance optimisation and deformation history interogation in engineering and geological materials. However, exploitations of texture are hampered by state-of-the-art characterisation techniques, none of which can routinely deliver the desirable non-destructive, volumetric measurements, especially at larger lengthscales. Here we report a direct and general methodology retrieving important lower-truncation-order texture and phase information from acoustic (compressional elastic) wave speed measurements in different directions through the material volume (avoiding the need for forward modelling). We demonstrate its deployment with ultrasound in the laboratory, where the results from seven representative samples are successfully validated against measurements performed using neutron diffraction. The acoustic method we have developed includes both fundamental wave propagation and texture inversion theories which are free from diffraction limits, they are arbitrarily scalable in dimension, and can be rapidly deployed to measure the texture of large objects. This opens up volumetric texture characterisation capabilities in the areas of material science and beyond, for both scientific and industrial applications.

1. Introduction

Crystallographic texture refers to the preferred orientation distribution of crystals in polycrystalline materials (e.g. metals, ceramics and minerals), which is normally developed during the thermo-mechanical deformation or recrystallisation processes [1,2]. It is a common phenomenon, with random or near-random texture relatively rare, especially in processed engineering materials [3]. Since most materials are anisotropic at the single crystal level, texture dominates many important macroscopic physical properties, such as thermal expansion of Zr cladding tubes in nuclear reactors [4], fatigue lives of titanium alloys in aero-engines [4], and strength of steels [1]. Given its origin, texture can also be used to infer the material's deformation histories, as is widely employed in geological mineral studies to deduce planetary dynamic evolution in Earth sciences [5–7].

The importance of texture has driven the developments of various characterisation techniques, and the established ones can be generally categorized as surface and bulk approaches. Prominent examples of the surface texture characterisation include lab-based X-ray [8] and Electron Back-Scattered diffraction (EBSD) [9], as well as the emerging Spatially Resolved Acoustic Spectroscopy (SRAS) based on surface acoustic waves [10]. These measurements are generally confined to localized, near surface (penetration depth < ~20 μm) inspections - where the texture can be unrepresentative of the bulk information due to the thermal-mechanical boundary conditions - and the latter two techniques also require elaborate surface preparations. The more desirable bulk texture can

* Corresponding author.
E-mail address: bo.lan@imperial.ac.uk (B. Lan).
[1] Now at: Department of Mechanical Engineering, Incheon National University, 119 Academy-ro, Incheon, 22012, Republic of Korea.

https://doi.org/10.1016/j.actamat.2018.08.037

only be measured using X-ray synchrotron and neutron diffraction [11], at national facilities with large-scale acceleration rings or nuclear reactors, such that access is normally rather limited. And even these techniques have difficulties penetrating thicknesses beyond millimetre-scales for metals (see Table 1 for a comparison of key attributes of these established techniques).

Due to their non-invasive nature, easy availability and transferability (e.g. to geophysics), acoustic (compressional elastic) waves, especially ultrasound (frequency > ~20 kHz), have been an attractive proposition to fulfil the important need of non-destructive, bulk texture evaluation. However, despite the fact that experimentally observed anisotropy of wave speeds have long been associated with texture [12], the inverse extraction of texture information from wave speeds has remained a difficult problem [13] that has not been satisfactorily solved. Prior pursuits of this capacity have been mainly based on guided ultrasound [14–19] (not bulk waves) in rolled plates with assumed orthorhombic sample symmetry simplifications (enforcing a number of the complex ODF coefficients to be 0 – four out of nine in the case of cubic material – and the remaining ones to be real), and the numerical optimisation procedure to obtain the reduced orientation distribution coefficients involves five-dimensional least-square fittings of a number of guided wave dispersion curves, with each point on these curves having to be iteratively searched. Therefore this process is highly cumbersome; and because of the least-square algorithm employed, the obtained texture solution can often be limited, inaccurate and non-unique. There have also been reports on the phenomenological texture-birefringence correlational observations [19,20], but they are not generic inversions either.

A theoretical solution to the inverse problem of extracting texture from acoustic wave speeds was given by the authors for both hexagonal [21] and cubic [22] crystal systems. It was revealed that mathematically, the wave speeds in a polycrystal can be expressed as a spherical convolution between texture and single crystal speeds, so that the recovery of texture information can be inversely achieved through a simple deconvolution process. This model has been primarily verified on different textures with the finite element modelling method, laying down the foundation for experimental studies. Very recently, studies utilising Resonant Ultrasound Spectroscopy (RUS) have employed the theoretical deconvolution in order to extract texture from elastic modulus measurements [23]. However, the direct extraction of texture from ultrasonic wave speeds has yet to be achieved, and this is the subject of the current work.

Here we seek to provide a comprehensive experimental validation of this wave speed approach. Through careful mechanical design, we establish a simple experimental platform based on the conventional ultrasonic scanning system, which is capable of measuring directional wave speeds required by the de-convolution process for volumetric texture. Ultrasonic examinations are performed on a range of industry-important hexagonal and cubic samples, and the retrieved texture information is validated against the well-established neutron diffraction technique. Good agreement is achieved between these techniques, and the acoustic method also offers an additional perspective on the phase compositions in dual-phase materials. As such, we hope this study bridges the gap from a tentative theory to trusted applications, thus marking down a milestone towards the development of a rapid, cheap, non-destructive and non-invasive characterisation tool for bulk texture measurement that could benefit many areas.

This paper is structured as follows: in section 2, we introduce the fundamental theoretical framework of the study, and discuss the experimental requirements it prescribes for texture inversion; in section 3 we describe in detail the experimental validation procedures, covering the ultrasonic wave speed measurement platform, the subject sample materials, as well as the neutron diffraction validation of the ultrasonic data. We then compare and discuss all the experimental results in section 4, including both texture and phase composition estimation. Finally, we discuss the significance and possible implications of the general methodology before concluding.

2. Theoretical basis: spherical convolution model

Assuming a polycrystalline aggregate is homogeneous in such a way that no matter in what directions an acoustic wave propagates through it, the wave always goes through the same texture, then the wave phase velocity variation function v in the three-dimensional (3D) space can be approximated by averaging the wave speeds along the propagation route from point to point, with the speed value at each point specified by its respective crystallographic orientation. This deduction leads to the expression of v as a generalized spherical convolution between the orientation distribution function (ODF) ω and the single crystal velocity variation function k (as the kernel function of the convolution, calculable from known single crystal elastic constants, SCECs), so that the spherical harmonic (SH) expansion coefficients of the three functions satisfy a point-wise multiplicative relationship [21,22]:

$$V_{lm} = \sum_{n=-l}^{l} W_{lmn} K_{ln} \tag{1}$$

where V_{lm} and K_{ln} are expanded with respect to the standard SH

Table 1
Comparison between the acoustic method in this study and five state-of-the-art texture measurement techniques, including lab-based X-ray [8], Electron Back-Scattered Diffraction (EBSD) [9], Spatially Resolved Acoustic Spectroscopy (SRAS) [10], X-ray synchrotron and neutron diffractions [11]. The technical advantages and wide applicability of the acoustic method are highlighted through the comparisons.

	Penetration depth	Sample preparation	Destructive?	Accessibility	Test time	Running Cost
Lab-based X-ray	surface	minimum	Yes	Widely available	Fairly fast	Fairly low
EBSD	surface	highly sophisticated	Yes	Widely available	Extremely slow	high
SRAS	surface	mirror-like surface finish	Yes	Limited	fast	Fairly low
X-ray synchrotron	bulk, up to cm scale for most metals	minimum	No, sample size up to what holder permits.	Limited	Test itself fast, but normally 6 month-1year waiting time	Extremely high
Neutron diffraction	bulk, up to cm scale for most metals	minimum	No, sample size up to what holder permits.	Limited	Test itself fast, but normally 6 month-1year waiting time	Extremely high
Acoustic method in this study	bulk and freely scalable, from mm (ultrasound) to km (seismic waves).	minimum	No, and potentially applicable directly to component level.	Most widely available	fast	Very low

bases $Y_{lm}(\theta,\phi)$ defined on the polar angle θ and azimuthal angle ϕ, while the ODF ω is expanded in terms of the Wigner-D function $D^{l}_{mn}(\alpha,\beta,\gamma)$ of the three Euler angles α,β,γ. In the case of the hexagonal crystal system, whose single crystal is transversely isotropic about its c-axis, the expression can be further simplified to be a convolution between the c-axis (i.e. (0002) pole) orientation distribution and the single crystal velocities [21]:

$$V_{lm} = W_{lm0}K_{l0} \tag{2}$$

Eqs (1) and (2) presents a remarkably simple homogenization model that can be used in both forward prediction of polycrystal wave speeds with known texture, and the inverse extraction of texture information from measured wave speeds. For the latter purpose, which is the focus of this paper, the ODF is recovered as its spherical harmonic (SH) expansions through a straightforward deconvolution process. This process is a generic inversion, since it involves only point-wise divisions of the SH expansion coefficients (no fitting is required), with no pre-assumed sample symmetry simplification, and the ODF SH coefficients are obtained as the unique solution [21] with high accuracy.

Here we apply this acoustic method on cubic and hexagonal crystal systems; the general convolution formulation also has the flexibility to incorporate transverse (shear) waves, which, combined with acoustic waves, could potentially allow inversion on less-symmetric crystal systems (such as tetragonal or orthorhombic).

The convolution model also reveals the limitation of the acoustic technique quantitatively. Since the wave speeds are derivatives of the 4th-rank elastic tensor and inherit the four-fold symmetry of the latter, the amplitudes of the single crystal terms K_{ln} rapidly diminish beyond the 4th expansion order, because the expansion bases represent similar levels of symmetry. As such, the influence of higher order ODF coefficients W_{lmn} on the polycrystal wave speed V_{lm} is negligible, and the texture that could be inversely retrieved from wave speeds (or from elasticity in general) is a truncation to the original up to the 4th order [21,22,24]. For hexagonal materials, an additional restriction is that the retrievable texture is only the distribution of the c-axes, as discussed in the introduction of Eq (2).

An important issue to point out is that the effects of residual stresses are neglected in both the theoretical deductions towards the convolution relationship and the experimental studies in this paper, because it has been previously demonstrated by both theoretical analysis [25] and experimental investigations [26,27] that their influences on the wave speeds are much smaller than those from texture, and their contributions are likely on par with experimental errors.

In practice, in order to retrieve the ODF SH coefficients W_{lmn}, the coefficients V_{lm} of the polycrystal wave speed in Eqs. (1) and (2) are calculated from speed values in discrete evaluation directions, by means of the Gaussian-Legendre numerical integration scheme [21,22]:

$$V_{lm} = \frac{\pi}{N}\sum_{i=0}^{2N-1}\sum_{j=0}^{N-1} v(\theta_i,\phi_j)Y^{*}_{lm}(\theta_i,\phi_j)\omega_N \tag{3}$$

where N is the order of the numerical integration scheme, θ_i denote the N number of discrete Gaussian-Legendre polar angles (nodes), ϕ_j are the 2N equi-angular azimuthal angles from 0 to 2π, $Y^{*}_{lm}(\theta_i,\phi_j)$ are the conjugates of the SH bases at (θ_i,ϕ_j) , and ω_N are the Gaussian weights of the nodes. For the targeted truncation order of 4 (W_{lmn} with $l \le 4$), $N = 6$ is enough to achieve the required numerical accuracy, and this in turn determines the 6 polar × 12 azimuthal directions in which wave speeds need to be measured experimentally, as shown in Fig. 1a. However, the wave speed's antipodal symmetry – wave travelling in opposite directions (e.g. two red arrows in Fig. 1a) have the same speed– can be utilized to halve the number of directions required. The obtained V_{lm} coefficients can then be used to construct the wave speed variation surface (e.g. in Fig. 1b) via SH synthesis, as well as in the deconvolution process to retrieve textures.

3. Experimental texture determination by ultrasound

3.1. Ultrasonic wave speed measurement platform

Eq. (3) effectively reduces the task of detecting texture into measuring the wave speeds in the propagation directions of Fig. 1a, and to achieve the full coverage of the directions, we have devised the simple experimental platform shown in Fig. 2a. Modified from Refs. [28] and [29], it is built on a conventional water-bath ultrasonic scanning system in routine non-destructive evaluation (NDE). Here the sample is immersed in water, and is subject to ultrasound signals propagated by a standard piezoelectric transducer, which acts both as the transmitter and receiver of the signals. As they go down along the water path and through the sample, the waves are refracted at both of the water-sample interfaces; and at the bottom of the water bath, the acoustic mirror reflects the down-going waves, sending them back upwards along exactly the same route as they went down, to be eventually received by the transducer. The refraction direction of the wave through the sample is adjusted by the combination of sample tilting and rotating (Fig. 2b), which result in shifts to the eventual arrival time of the reflected signals at the transducer; and by correlating them with the times of the normal-incident cases, both the refraction direction and velocity of the wave can be calculated simultaneously [28,29].

The through-thickness transmission of ultrasound ensures the inspections of the average macro-texture across a volumetric region of interest (VROI), which is assumed to be homogeneous as per the premises of the theoretical convolution (and indeed of bulk diffraction techniques such as neutron). The validity of this homogeneity assumption will be investigated later on our samples. Note that while we only make use of the compressional waves through the sample for texture detections here, the oblique incident waves on the water-solid interface can also induce transverse waves, which are observable using the setup [28].

3.2. Examined materials and sample preparation

Seven samples of three material types are examined experimentally, including one body-centred cubic (BCC) and two face-centred cubic (FCC) stainless steels (SS), three hexagonal close-packed (HCP) samples of Ti and Zr, and one HCP-BCC dual-phase sample of the Ti-6Al-4V alloy. The grades of the BCC, FCC-1 and FCC-2 SS samples are respectively 430 (ferritic), 304 and 316 (both austenitic), and the HCP-1, 2, and 3 samples are commercially pure (CP) Ti, CP Zr and Zircaloy-4. These materials are pivotal in civil engineering (SS) [30], aerospace (Ti) [4,31], and nuclear (Zr) [4] industrial applications [32], and are representative of the broad applicability of the acoustic measurement methodology to the likes of metals, ceramics and minerals.

Two of these samples (HCP-3 and Ti-6Al-4V) were provided by our research partner, a major UK manufacturing company, and all the others were purchased directly from metal suppliers. The three HCP and the HCP-BCC samples were in the shapes of 5–7 mm thick plates, while the three SS ones were 2–3 mm sheets. The samples were cut into 85 mm-across coupons using electrical discharge machining (EDM, which does not involve plastic deformation, hence does not alter local textures) to fit into holders for ultrasonic tests.

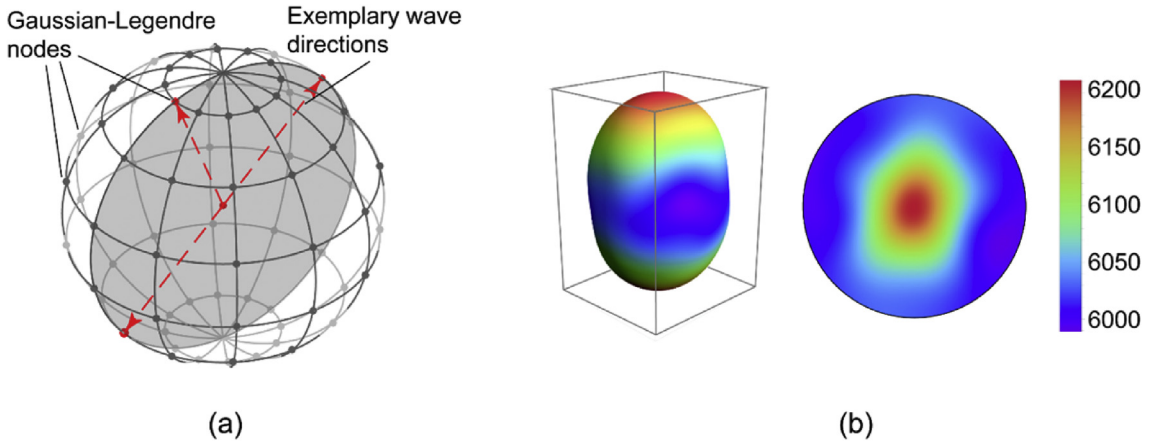

Fig. 1. Acoustic wave speed surfaces constructed via numerical integration. (a). Directions in which wave speeds are required by the Gaussian-Legendre quadrature to be measured (partly reproduced from Ref. [23]). Note the antipodal symmetry (i.e. reciprocity) which halves the number of directions needed; (b). Exemplary wave speed surface reconstructed from discrete measurements, shown as explicit 3D plot (left) and its corresponding stereographic projection (right).

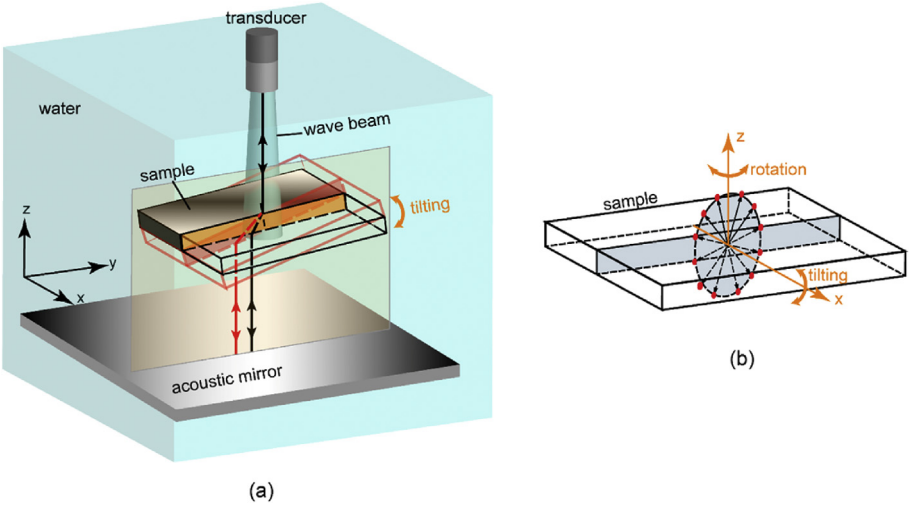

Fig. 2. The experimental platform for measuring directional ultrasonic wave speeds. (a). Schematic of the setup which is constructed upon a conventional water-bath system. Its through-transmission of ultrasound enables measurements of average bulk texture across the VROI. (b). Adjustments of the wave refraction direction through the sample by combination of sample tilting (rotation about x) and rotating (about z) to cover all directions needed.

Minimal surface preparation is required for our ultrasonic setup, as the paramount requirements to ensure experimental wave speed measurement accuracy are the parallelism and flatness of the sample surfaces, rather than their finish. The conditions of the commercially available rolled plates and sheets (<20 μm parallelism, while surface roughness can be as large as ~30 μm) are generally sufficient. In fact, six out of the seven samples were examined in as-received conditions, and the one sample needed machining (Ti-6Al-4V) only because it was initially supplied in a wedge shape.

3.3. Ultrasonic scans: homogeneity studies and texture measurements

The assumption that a polycrystal is directionally homogeneous is fundamental to the texture inversion theory, and its validity within the bulk of real-world samples was investigated via two types of experiments: normal incident scans within a single VROI, and full 3D velocity measurements on spatially resolved regions.

Normal scans can indirectly reflect the level of macro-texture inhomogeneities within a VROI that would otherwise cause noticeable angular and normal velocity fluctuations. Tests were performed on one Ti and two different Ti-6Al-4V samples, and the results in Fig. 3a show little wave speed variation, with the standard deviations lower than the estimated noise level (~5–10 m/s), indicating little to no inhomogeneity which is significant enough to affect wave propagations within the regions.

Full 3D wave speed examinations at spatially resolved locations were carried out to investigate such variations over larger length-scales. A pair of coupons were cut at far-apart positions (>150 mm) from three plates of Ti, 304 SS and Ti-6Al-4V, and almost identical patterns of the wave speed surfaces were obtained for all pairs in Fig. 3b (though inevitably with small differences of velocity values). These results demonstrate that even across these larger length-scales, no significant spatial variation in either texture or homogeneities are observable by ultrasound, which in turn strengthens the assumption within the much smaller VROIs. In addition, it is worth noting that the homogeneity assumption (on the macroscopic level) is a relatively relaxed one for such 3D measurements: e.g. a layered plate is technically inhomogenous, but it would still

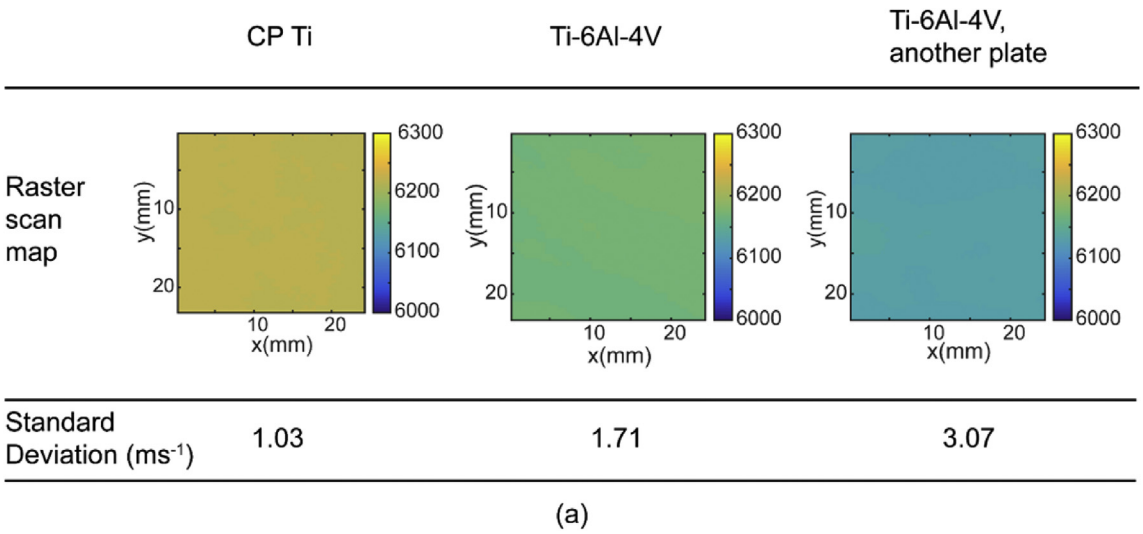

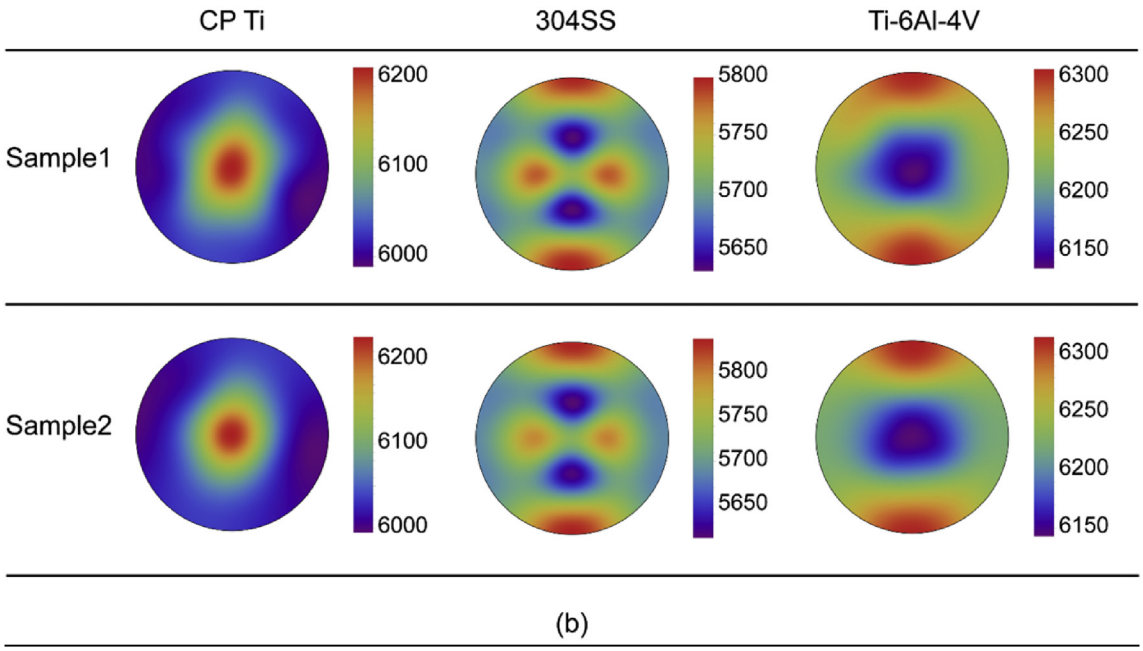

Fig. 3. Homogeneity investigation results on some of the examined samples. (a). Normal-incident wave speed scan results on three samples across the typically sized VROI; (b). Full 3D wave speed surfaces of three pairs of samples cut from locations far apart (>150 mm) on the same plates (partly reproduced from Ref. [23]).

satisfy the directional homogeneity and is fit for the texture inversion, when evaluated in the discrete directions of Fig. 1a.

These investigations also confirm the robustness of the ultrasonic platform in measuring wave speeds in spite of some particular micro-structural inhomogeneities that are present in these samples. For example, EBSD scans on the Ti-6Al-4V sample (a representative one shown in Fig. 4) revealed that they in fact contained many localized inhomogeneities termed macrozones [33] (or micro-textured regions, MTRs), which are clusters of large numbers (often >100 on a 2D section) of neighbouring grains with similar orientations. Ultrasound can still reliably measure these samples because of the propagation mechanics of acoustic waves: they tend to overlook micro-structural features that are smaller than their wavelengths and reflect only the overall macroscopic elasticity. This property can be exploited in combination with the scalability of the convolution model: since the theory is independent of frequency/wavelengths, higher frequencies can be normally used to achieve better spatial and temporal resolution; when encountering waveform distortions or amplitude attenuations that are likely to be caused by micro-structural features, one can then resort to lower frequencies (i.e. larger wavelengths) to maintain the reliability of the measurements.

With the basic premises confirmed, we proceed to the most important texture measurements with ultrasound. 10 MHz waves generated by a standard non-focused transducer were used for these tests; the wavelengths are typically >10 times the grain sizes, enabling the waves to propagate through the polycrystals with little scattering and achieve excellent signal to noise ratios (normally >~40 dB). The through-thickness VROI at the centre of each sample was examined, whose width is the larger one of either ~5

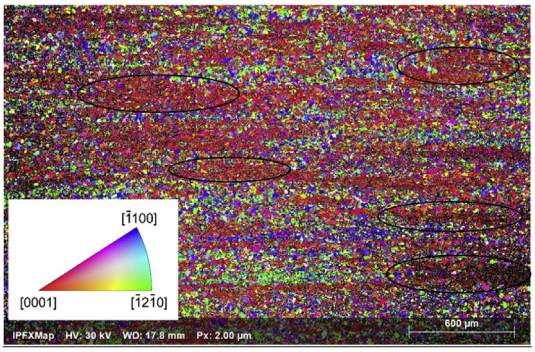

Fig. 4. EBSD scan of a region on a through-thickness section of the Ti-6Al-4V sample showing the presence of macrozones (MTRs). Our acoustic method is robust against such micro-structural inhomogeneities.

times the sample thickness, as inscribed by the largest refraction angle of the Gaussian-Legendre nodes, or the ultrasound beam spreading size at the transducer-sample distance, and is estimated to be ~20 mm across for our configuration. With typical grain sizes of 20–50 μm for the samples, the average texture of the VROI can contain statistical counts of as many as $>10^8$ crystals. Each sample was tested 3–4 times by ultrasound, and the wave speed results were averaged to reduce experimental errors. As mentioned, the error and repeatability level of the ultrasonic wave speed measurements were estimated to be 5–10 m/s, which were much smaller compared to often >150 m/s differences caused by texture.

After obtaining the measurements in all Gaussian-Legendre directions, the texture inversion was performed through simple data processing procedures. The discrete velocity values were firstly used in the numerical integration Eq. (3) to calculate the SH expansion coefficients V_{lm}, which were then input to the spherical convolution equation (1) or (2) to obtain ODF coefficients W_{lmn} using known single crystal K_{ln} values (the SCECs used to calculate K_{ln} are listed in Appendix Table A.1). These W_{lmn} values were ready for the software toolbox MTEX [34] to reconstruct the (truncated) ODF and plot out the pole figures.

3.4. Neutron diffraction texture validations: monochromatic over TOF

These acoustic textures were verified against neutron diffraction measurements performed on the STRESS-SPEC instrument [35] at FRM II, Heinz Maier-Leibnitz Zentrum (MLZ), Germany. The VROIs were cut out through-thickness into 20 mm-diameter cylinders by electric discharging manufacturing, and were mounted on a conventional Eulerian goniometer, with the full bulk volumes exposed to illuminations by a monochromatic neutron beam, thus ensuring the detection of exactly the same texture across the same volumetric regions as had been done using the ultrasound.

During the diffraction tests, both the incident neutron beam direction and the detector position were fixed, and the goniometer rotated the mounted sample to cover the full 3D orientations. At each sample orientation, the crystallographic plane (pole) that satisfied the Bragg's Law reflected the beam to the detector, and the received beam intensities, which were obtained by integrating the recorded diffraction peak profiles using the software StressTextureCalculator [36], were proportional to the volume fraction of crystals with the crystallographic plane correctly aligned. Pole figures were directly plotted from such intensities, and the classic inversion process was then performed to calculate the ODF from multiple pole figures [37,38]. Both of these processes were done in the MTEX toolbox [34].

Note that both the monochromatic and time-of-flight (TOF) variants of neutron diffraction tests were performed and compared on some of our samples, and the monochromatic technique was selected as more suitable verification for our ultrasound measurements, since its texture data is directly reconstructed from diffraction intensities of monochromatic beams. Unfortunately, we had difficulties with our samples for the Rietveld analysis of TOF data, and were unable to obtain satisfactory texture results by following the standard routines in literature [39,40]. A more detailed description of the TOF measurements on our samples and their comparisons against the monochromatic results is available in Appendix 2.

4. Experimental results

In this section, results of experimentally determined texture by ultrasound are presented and compared with neutron results for all samples, and a simple estimation of phase compositions in dual-phase materials is demonstrated using Ti-6Al-4V as an example.

4.1. Cubic materials

The (111) and (200) pole figures of the three cubic samples by both detection techniques are plotted in Fig. 5, with the neutron results also truncated to the same 4th-order for direct comparisons with ultrasound. It is evident that both the overall distribution patterns and the intensities of the pole figures generally agree well between the acoustic and truncated neutron results, confirming experimentally the postulated convolution between the lower-order texture coefficients and wave speeds. These agreements are remarkable considering the multiple factors that could have had negative influences on them, such as inaccurate SCECs and diffraction peak intensity calculations (e.g. peak integration regions are hand-selected in post-processing, so even the same data set could end up with slightly different pole figures). These factors may have contributed to the FCC-2 sample's slightly more pronounced differences, where the texture intensities are relatively weak in the first place. Here we define a numerical metric, the Relative Distance (RD):

$$\oint_{\Omega} |(\omega_{Acoust} - \omega_{TruncNeutron})| d\Omega \Big/ \oint_{\Omega} |\omega_{TruncNeutron}| d\Omega \tag{4}$$

(where ω refers to ODF) to quantify the differences between these two texture results, and the RD values are respectively 7.1% (−52.9 dB), 8.0% (−50.8 dB) and 6.9% (−53.5 dB) for the samples. These agreements confirm that the de-convolution process has been successful.

Comparisons with the full neutron results render some contrasts: while all three pole figure pairs agree well for the BCC SS, the acoustic and truncated figures of the two FCC samples appear different from the full neutron texture. These differences, evident in Fig. 5, are probably due to the textures of these particular samples, where the more symmetric plastic deformation mechanisms [2] (via {111}<110> slip) of the FCC crystal system have introduced more significant higher-order ODF terms during the deformation processes. These terms qualitatively impact visual inspection of the pole figures when different truncation levels are applied.

However, the significances of the acoustic texture should be emphasized. Many typical FCC texture types, such as Cube, Goss and Brass, do not suffer from this issue as notably as the FCC-1 and 2 samples, and can be represented reasonably well after truncation (as demonstrated in Appendix 3. Moreover, it is well-known that the polycrystal elasticity and many other properties that can be

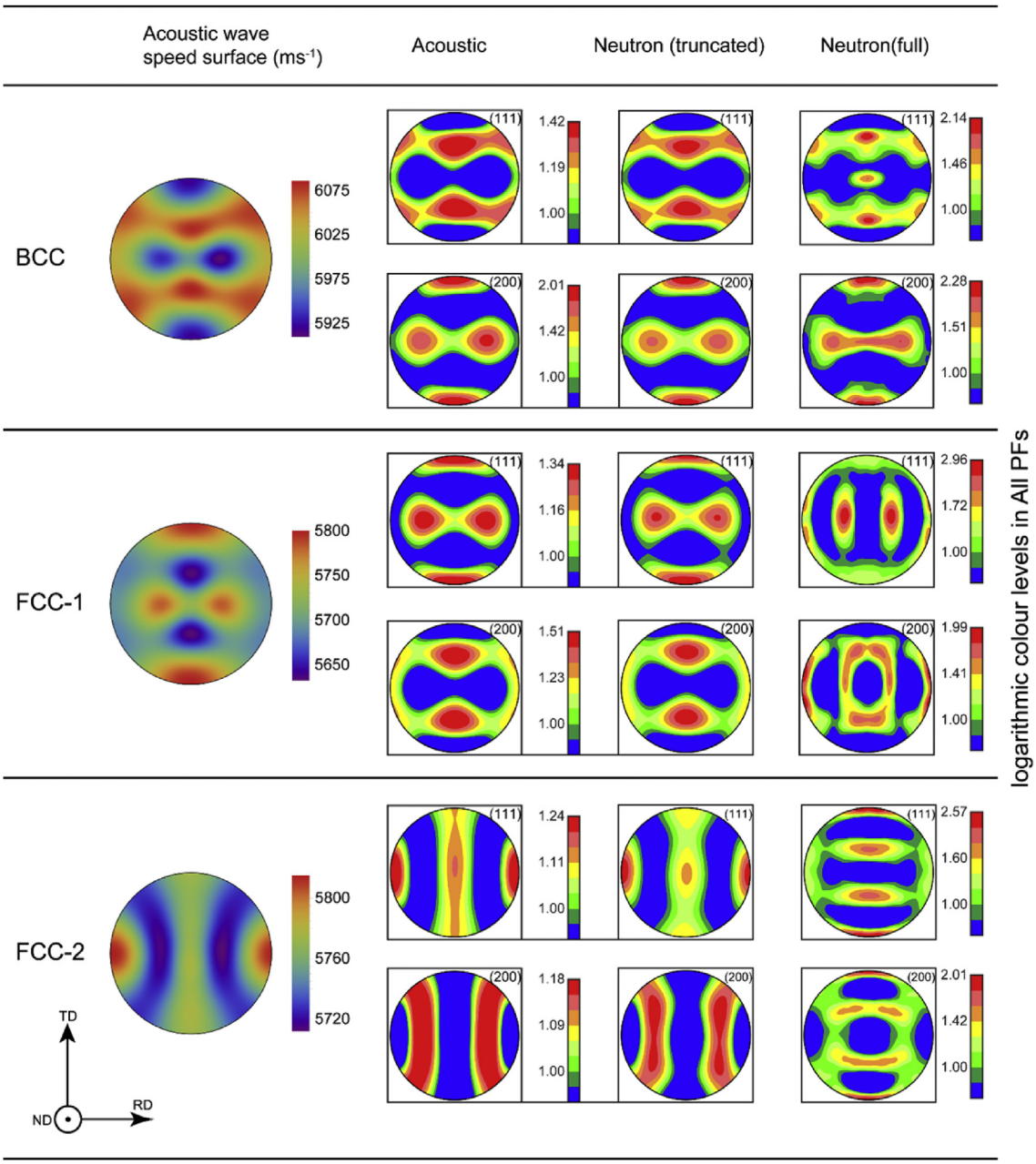

Fig. 5. Experimental results of the three cubic samples. Wave speed surfaces are plotted alongside pole figures obtained from acoustic and neutron examinations, with neutron results also truncated to 4th SH order. The sample system is defined by the rolling direction (RD), transverse direction (TD) and normal direction (ND). FCC-1 results partly reproduced from Ref. [23].

described by tensors of lower than 4th ranks (including magnetism, thermal expansion —isotropic for cubic materials, but important for hexagonal ones, e.g. Zr, and piezoelectricity), depend most strongly upon the lower-order ODF coefficients and the terms beyond 4th-order are of minimal or no consequence [21–23]. For these properties, the acoustic pole figures could even be more usefully representative, since incorporating the higher-order terms may provide misleading qualitative interpretations (e.g. the full neutron ones in Fig. 5). Finally, the FCC crystal's symmetric deformation mechanisms also indicate SH terms that are potentially numerically related, so that empirical links may be established to infer full textures and structural evolutions from the truncated acoustic ODFs.

4.2. Hexagonal materials

The acoustic technique also delivers pole figures of the three HCP samples in Fig. 6. Again, there is successful agreement between the acoustic and truncated neutron results, with good reproduction of both qualitative distribution patterns and quantitative intensity levels, and the RDs are 17.7% (−35.32 db), 12.6% (−41.43 db) and 18.0% (−34.33 db) respectively. Good numerical agreements are also achieved in calculating the industry-relevant Kearns factors [41], which describe the proportions of c-axes aligned along the principal sample coordinates.

The full neutron pole figures are also well represented by the acoustic results in Fig. 6, displaying only mild losses of local sharpness, and minor discrepancies of intensities. The absence of

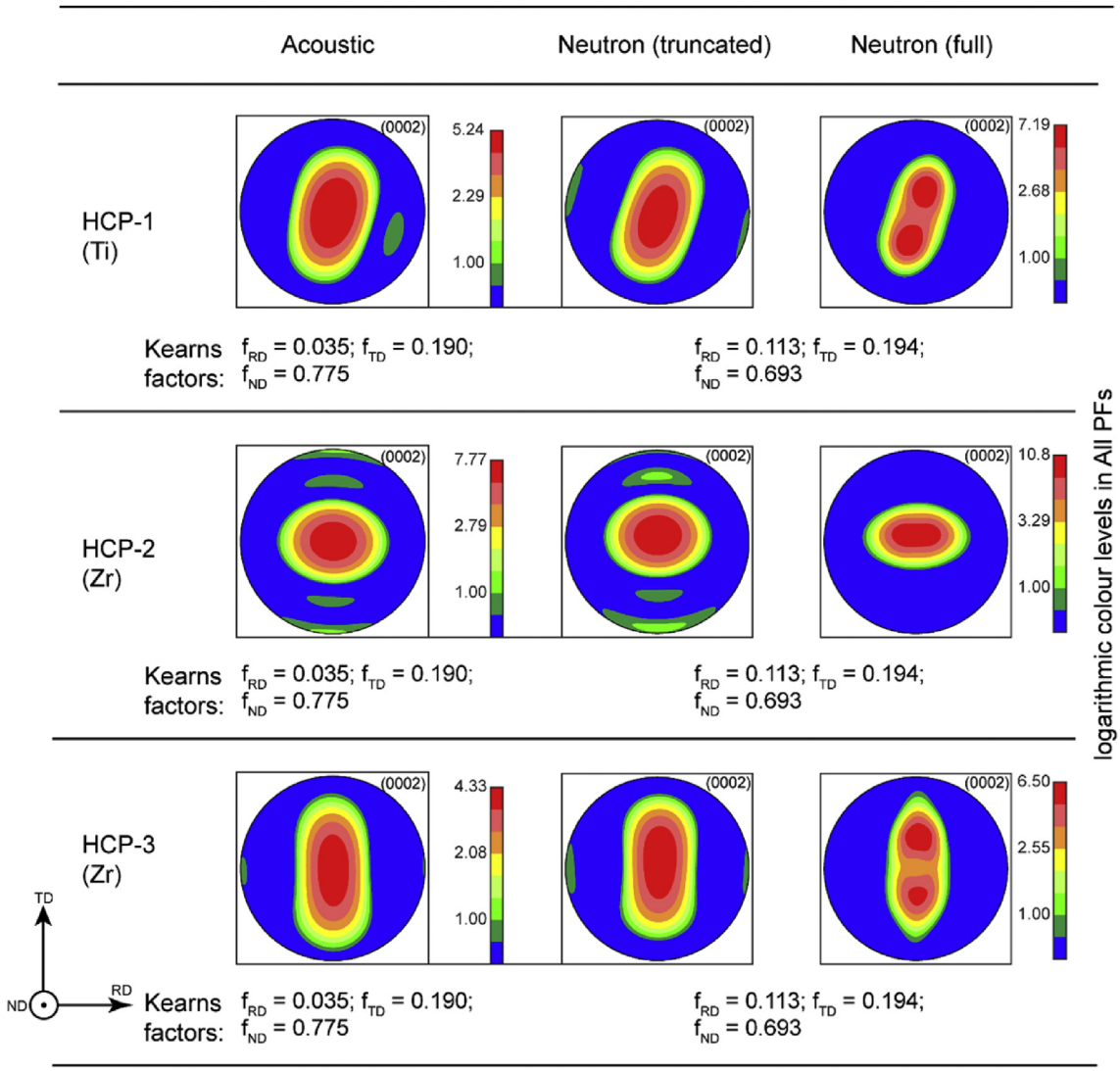

Fig. 6. Results of the three HCP samples from acoustic and neutron techniques. Kearns factors, which describe proportions of c-axes along three sample directions, show good quantitative agreements. Note that they only depend on ODF up to 2nd-order [41], so are not affected by the truncation. HCP-1 results partly reproduced from Ref. [23].

localized higher-order features, as discussed, does not impair the method's ability to capture important distributions, nor to predict many important physical properties. And the intensities are, by definition, merely indicators of orientation distribution preference levels compared to random texture (where the intensity is equal to 1 everywhere). The acoustic results still illustrate such preference of distribution clearly; and given that their numerical values are strongly (though nonlinearly) correlated with the full intensities, the acoustic results could be empirically scaled to reflect the latter.

Fig. 7 shows the pole figure results of the cross-rolled, HCP-BCC dual-phase Ti-6Al-4V sample. In this case, the material's BCC beta phase, which is of ~10% volume fraction [31,42], is a source of uncertainty and is treated differently between the techniques. The acoustic method assumed the beta phase to be elastically isotropic (i.e. with no texture), and ascribes all wave speed anisotropy to the dominant HCP alpha phase. The alpha texture is determined accordingly; while the neutron diffraction was unable to differentiate the overlapping (0002)|alpha-(110)|beta diffraction peaks (as per the Burgers' Orientation relationship) [31,42], and the beta (002) peak was too weak to be clearly distinguished from noise, so it instead regarded intensities at the (0002) Bragg angle as entirely alpha-phase contributions (for reference, the TOF neutron method is not able to provide certainty on the beta phase either, see Appendix 2). These different treatments led to some intensity discrepancies of the pole figures, with neither result being perfectly accurate, but the qualitative distributions still agree well, with both cross-rolling directions and the stronger intensities in the transverse direction (TD) clearly identified.

4.3. Phase estimation in dual-phase materials

The acoustic approach offers an additional important perspective into material phase compositions, for which the 0th-order polycrystal SH term V_{00} holds the key. According to the convolution, the polycrystal V_{00} term is linked to the single crystal term K_{00} by the ODF's 0^{th}-order coefficient W_{000}:

$$V_{00} = W_{000}K_{00} \tag{5}$$

W_{000} is always equal to 1 regardless of the texture, so the V_{00} value in a single phase material is always equal to K_{00}, and is an intrinsic feature of the phase reflecting acoustic properties and the

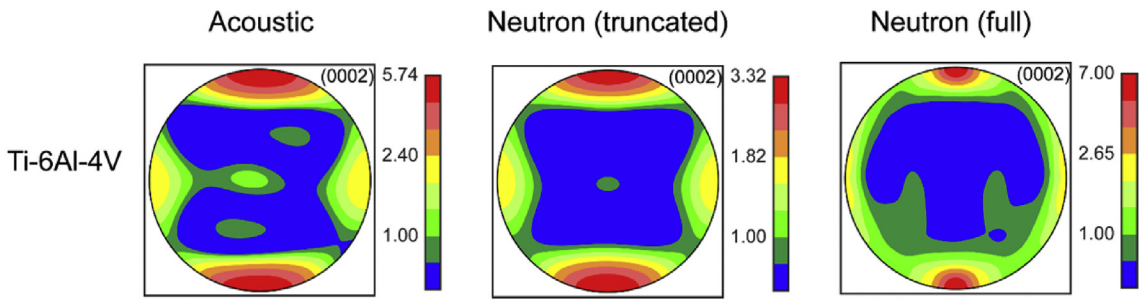

Fig. 7. PFs of the cross-rolled HCP-BCC dual-phase sample (partly reproduced from Ref. [23]). The different treatments of the beta phase in data post-processing caused discrepancies in PF intensities, but the qualitative distributions still agree well.

SCEC accuracies. In dual-phase materials, the overall V_{00} value of the polycrystal can be approximated by the simple volume fraction average of the two phases' K_{00} values. For example, if the fraction of the alpha phase is denoted as h, then we have:

$$V_{00}|_{overall} = h \times V_{00}|_{alpha} + (1-h) \times V_{00}|_{beta} \quad (6)$$

With $V_{00}|_{alpha}$ and $V_{00}|_{beta}$ values again deductible from known SCECs, the experimentally measured $V_{00}|_{overall}$ provides a simple arithmetic estimation of h inversely. Our Ti-6Al-4V sample, for instance, has alpha-phase $K_{00} = 22091.9$ and beta $K_{00} = 21617.6$ (from SCECs in Ref. [42]), with measured polycrystal $V_{00} = 22029.2$, yielding an estimated alpha percentage of 86.8%, which is reasonably close to the ~90% data in literature [31,42].

The precision of the estimation is subject to the accuracies of the SCECs and experimentally measured V_{00} values, the latter of which is investigated here on its repeatability and accuracy. The repeatability can be studied via the three pairs of samples in Fig. 3b. After multiple tests, the experimental V_{00} values of these samples calculated from the average speeds are listed in Table 2, and excellent repeatability for the measurement of this value is observed. As for accuracies, the V_{00} values are basically the average speed of all directions multiplied by a factor of $\sqrt{4\pi}$. For an estimated experimental accuracy of ~5–10 m/s in individual directions (though V_{00} is the average of 36 directional velocities, so theoretically should have smaller error levels), the V_{00} value has an uncertainty of ±17.5–35.5. In the case of Ti-6Al-4V, whose alpha and beta V_{00} values are 474.3 apart (22091.9 and 21617.6 respectively), this translates into ± 4–7% uncertainty in the estimated phase composition. Apparently, this estimation is also dependent on the material properties (e.g. how far apart the V_{00} values of alpha and beta phases are).

Despite such dependences, there is, in many cases (e.g. Ti-6Al-4V), no other non-destructive technique for bulk phase composition measurements, so the acoustic method could emerge as a useful tool for structural characterisation. It works well against micro-structual inhomogeneity (again in the case of Ti-6Al-4V), and may be used for absolute-term estimations as well as relative-term monitoring of changes between samples.

Table 2
Experimental repeatability of measuring V_{00} values in the three pairs of samples shown in Fig. 3b.

Material	CP Ti	304 SS	Ti-6Al-4V
V_{00} value of sample 1	21518.0	20253.6	22029.2
V_{00} value of sample 2	21526.2	20272.3	22027.6
Difference	7.8	18.7	1.6

5. Discussions

The ultrasound setup in Fig. 2 has proved the convolution methodology to be a reliable and accurate way of measuring bulk texture, on a range of industry-important hexagonal and cubic materials. This setup can be easily integrated to the existing industrial ultrasonic scanning systems; if fully automated, it is estimated to reduce the testing time to a couple of minutes per location, providing significant improvements in efficiency compared to current standard practices such as EBSD (which takes hours for similar, millimetre-scale surface inspections). And given the wide and cheap availability of the ultrasonic equipment, this could transform the capability of non-destructive, volumetric measurements of texture - desirable yet currently only achievable via neutron/synchrotron at national facilities - into routine checks on production lines and in research laboratories. The rapid feedback loop of texture information, as well as its resultant physical anisotropy, could enable considerably better control over material performances and fabrication efficiencies in mechanical metallurgy and manufacturing of materials.

Furthermore, the wave propagation and texture inversion theories underpinning our method are dimensionless – meaning that they are arbitrarily scalable in dimension, and are equally applicable across the frequency spectrum. Therefore, the power of this general methodology extends beyond the specific setup in Fig. 2, such that any other alternative transduction setup capable of measuring the arrival time of ultrasound through the bulk of a material sample from one point to another would be equally suitable. For example, an experimental implementation [23] based on Resonant Ultrasound Spectroscopy has recently been proved capable of achieving similar texture measurements by indirectly retrieving elasticity from vibrational resonances. Other alternative setups at this spatial scale could use piezo-electric point-contact transducers or ultrasonic array transducers, setups at smaller spatial scale could use laser-ultrasound excitation and laser interferometer reception, and setups at larger scale could use seismic sources and accelerometer receivers. The approach to sampling, acquisition and processing for inversion would be the same for any of these other example setups. The scalability also amplifies an additional advantage of the acoustic approach, namely its great penetrating power: e.g. while even neutron or X-ray synchrotron would struggle to penetrate metal samples beyond 10 mm thick, a common ultrasound equipment can easily evaluate those of >50 mm thicknesses.

It appears reasonable to further postulate that the scalability could even extend applications of the general methodology beyond material sciences, into the realm of Earth science, given that the fundamental propagation mechanisms of seismic waves in minerals are the same as ultrasound in metals. This could for example enable deployments of kilometre seismic waves - and a plethora of

intermediate-scale ones - as large-scale tools for probing textures in ice (hexagonal) under natural conditions for understanding of glacier flows [5]; and in deep Earth [43] for interpretations of planetary structures and their dynamic evolutions. The phase composition estimation could also be of value, e.g. for interpreting the phases of the Earth's inner core [43] from seismic anisotropies, as our understanding of its thermodynamic conditions and chemical compositions advances. However, stiff challenges should be expected for these much less controlled explorations (and also for industrial applications under extreme conditions, e.g. steels at high temperatures [44]), including high levels of anisotropy and inhomogeneity of the materials, as well as limited angular accessibilities.

6. Conclusion

As an important validation of a general convolution approach to extract texture information from acoustic wave speeds, an experimental platform that is capable of measuring the angular variation of ultrasound within a volumetric region has been established, based on a conventional system that is used in non-destructive evaluation. High-fidelity texture information of seven industrially-significant hexagonal and cubic (both BCC and FCC) samples, including Ti, Zr and stainless steel, were recovered from ultrasonic measurements, and were successfully verified against the well-established monochromatic neutron diffraction technique. Besides the excellent agreements between the techniques for all the samples, possible reasons for the different visual inspections of pole figures observed on FCC samples (truncation of harmonics) were discussed. In addition, the acoustic method offers an important perspective on the phase composition of dual-phase materials, which was successfully demonstrated using Ti-6Al-4V as an example.

As such, the present work establishes the general methodology as an exciting new characterisation tool to non-destructively identify the orientation and phase distributions of crystals within volumetric regions. Its successful demonstration on the representative samples implies the methodology's wider potential extending beyond engineering metals, to ceramics and geological minerals, and its impact could be expected across various research areas and industries.

Data statement

MTEX scripts and the texture data are provided in the supplementary data for readers who wish to explore alternative representations of the textures.

Acknowledgements

This work is part of the HEXMAT programme funded by the Engineering and Physical Sciences Research Council (EP/K034332/1). The authors acknowledge the financial support provided by FRM II for neutron scattering measurements at the Heinz Maier-Leibnitz Zentrum (MLZ), Garching, Germany, and the GEM neutron facility at ISIS, Rutherford Appleton Laboratory, UK. B.L. wishes to thank Dr. W. Kockelmann of GEM, Dr. A. Pilchak of US Air Force, Dr V. Miller of University California, Santa Barbara, Prof. R. Craster, Dr V Tong, S. Wyatt and Dr M.-S. Pham of Imperial College, Prof. D. Rugg of Rolls-Royce plc., Prof A. Rollett of Carnegie Mellon University and Dr A. Creuziger of National Institute of Standards and Technology for help at various stages of the study. F.P.E.D acknowledges the Royal Academy of Engineering (RAEng) chair at Imperial College, and T.B.B. acknowledges the RAEng fellowship. All authors would also like to thank colleagues Dr. C. Gourlay and Prof. S. Maier at Imperial for commenting on the draft of the paper before submission.

Appendix A. Supplementary data

Supplementary data related to this article can be found at https://doi.org/10.1016/j.actamat.2018.08.037.

References

[1] U.F. Kocks, H.-R. Wenk, C.N. Tomé, Texture and Anisotropy : Preferred Orientations in Polycrystals and Their Effect on Materials Properties, Cambridge University Press, 2000.
[2] H.-R. Wenk, P. Van Houtte, Texture and anisotropy, Rep. Prog. Phys. 67 (2004) 1367.
[3] O. Engler, V. Randle, Introduction to Texture Analysis : Macrotexture, Microtexture, and Orientation Mapping, CRC Press, 2010.
[4] Y. Wang, J. Huang, Texture analysis in hexagonal materials, Mater. Chem. Phys. 81 (2003) 11–26.
[5] K. Bennett, H.-R. Wenk, W.B. Durham, L.A. Stern, S.H. Kirby, Preferred crystallographic orientation in the ice I ← II transformation and the flow of ice II, Philos. Mag. A Phys. Condens. Matter, Struct. Defects Mech. Prop. 76 (1997) 413–435.
[6] H.-R. Wenk, Preferred Orientation in Deformed Metals and Rocks : an Introduction to Modern Texture Analysis, Academic Press, 1985.
[7] B.S.G. Almqvist, D. Mainprice, Seismic properties and anisotropy of the continental crust: predictions based on mineral texture and rock microstructure, Rev. Geophys. 55 (2017) 367–433.
[8] B.E. Warren, X-ray Diffraction, Dover Publications, 1969.
[9] A.J. Schwartz, M. Kumar, B.L. Adams, D.P. Field, Electron Backscatter Diffraction in Materials Science, Springer US, 2000.
[10] S.D. Sharples, M. Clark, M.G. Somekh, Spatially resolved acoustic spectroscopy for fast noncontact imaging of material microstructure, Optic Express 14 (2006) 10435–10440.
[11] A. Schreyer, H. Clemens, Neutrons and Synchrotron Radiation in Engineering Materials Science: from Fundamentals to Applications, John Wiley & Sons, 2017.
[12] R.B. Thompson, S.S. Lee, J.F. Smith, Angular dependence of ultrasonic wave propagation in a stressed, orthorhombic continuum: theory and application to the measurement of stress and texture, J. Acoust. Soc. Am. 80 (1986) 921–931.
[13] C.M. Sayers, Ultrasonic velocities in anisotropic polycrystalline aggregates, J. Phys. D Appl. Phys. 15 (1982) 2157–2167.
[14] M. Hirao, K. Aoki, H. Fukuoka, Texture of polycrystalline metals characterized by ultrasonic velocity measurements, J. Acoust. Soc. Am. 81 (1987) 1434.
[15] R.B. Thompson, S.S. Lee, Y. Li, C.M. Sayers, Ultrasonic and neutron diffraction characterization of texture in an inhomogeneously rolled titanium plate, Mater. Sci. Eng. A. 177 (1994) 261–267.
[16] R.B. Thompson, J.F. Smith, S.S. Lee, G.C. Johnson, A comparison of ultrasonic and X-ray determinations of texture in thin Cu and Al plates, Metall. Trans. A. 20 (1989) 2431–2447.
[17] A.J. Anderson, R.B. Thompson, C.S. Cook, Ultrasonic measurement of the kearns texture factors in zircaloy, zirconium, and titanium, Metall. Mater. Trans. A. 30 (1999) 1981–1988.
[18] S. Dixon, C. Edwards, S.B. Palmer, Texture measurements of metal sheets using wideband electromagnetic acoustic transducers, J. Phys. D Appl. Phys. 35 (2002) 816–824.
[19] S. Hirsekorn, E. Schneider, Characterization of rolling texture by ultrasonic dispersion measurement, in: Nondestruct. Charact. Mater. Proc. 3rd Int. Symp. Saarbrücken, FRG, Oct. 3-6, 1988, Springer, n.d.: p. 289.
[20] S.P. Sagar, B.R. Kumar, S.G. Chowdhury, P.K. De, R.N. Ghosh, Determination of crystallographic texture in cold-rolled copper and stainless steel by spectrum analysis of ultrasonic signal, Scripta Mater. 58 (2008) 595–598.
[21] B. Lan, M.J.S. Lowe, F.P.E. Dunne, A spherical harmonic approach for the determination of HCP texture from ultrasound: a solution to the inverse problem, J. Mech. Phys. Solid. 83 (2015) 179–198.
[22] B. Lan, M.J.S. Lowe, F.P.E. Dunne, A generalized spherical harmonic deconvolution to obtain texture of cubic materials from ultrasonic wave speed, J. Mech. Phys. Solid. 83 (2015) 221–242.
[23] B. Lan, M.A. Carpenter, W. Gan, M. Hofmann, F.P.E. Dunne, M.J.S. Lowe, Rapid measurement of volumetric texture using resonant ultrasound spectroscopy, Scripta Mater. 157 (2018) 44–48.
[24] H.-J. Bunge, Texture Analysis in Materials Science: Mathematical Methods, Elsevier, 2013.
[25] R.N. Thurston, Effective elastic coefficients for wave propagation in crystals under stress, J. Acoust. Soc. Am. 37 (1965) 348–356.
[26] D.M. Egle, D.E. Bray, Measurement of acoustoelastic and third-order elastic constants for rail steel, J. Acoust. Soc. Am. 60 (1976) 741–744.
[27] G.C. Johnson, On the applicability of acoustoelasticity for residual stress determination, J. Appl. Mech. 48 (1981) 791.
[28] S.I. Rokhlin, W. Wang, Double through-transmission bulk wave method for ultrasonic phase velocity measurement and determination of elastic constants of composite materials, J. Acoust. Soc. Am. 91 (1992) 3303.
[29] Y.C. Chu, S.I. Rokhlin, Comparative analysis of through-transmission ultrasonic

bulk wave methods for phase velocity measurements in anisotropic materials, J. Acoust. Soc. Am. 95 (1994) 3204.
[30] D.T. Llewellyn, R.C. Hudd, Steels : Metallurgy and Applications, Butterworth-Heinemann, 1998.
[31] G. Lütjering, J.C. Williams, Titanium, Springer Berlin Heidelberg, 2007.
[32] K. Lu, The future of metals, Science 328 (2010) 319–320.
[33] K. Le Biavant, S. Pommier, C. Prioul, Local texture and fatigue crack initiation in a Ti-6Al-4V titanium alloy, Fatig. Fract. Eng. Mater. Struct. 25 (2002) 527–545.
[34] F. Bachmann, R. Hielscher, H. Schaeben, Texture analysis with MTEX – free and open source software toolbox, Solid State Phenom. 160 (2010) 63–68.
[35] H.-G. Brokmeier, W.M. Gan, C. Randau, M. Völler, J. Rebelo-Kornmeier, M. Hofmann, Texture analysis at neutron diffractometer STRESS-SPEC, Nucl. Instruments Methods Phys. Res. Sect. A Accel. Spectrometers, Detect. Assoc. Equip. 642 (2011) 87–92.
[36] C. Randau, U. Garbe, H.-G. Brokmeier, *StressTextureCalculator* : a software tool to extract texture, strain and microstructure information from area-detector measurements, J. Appl. Crystallogr. 44 (2011) 641–646.
[37] R. Roe, Description of crystallite orientation in polycrystalline materials. Iii. General solution to pole figure inversion, J. Appl. Phys. 36 (1965) 2024–2031.
[38] R. Roe, Inversion of pole figures for materials having cubic crystal symmetry, J. Appl. Phys. 37 (1966) 2069–2072.
[39] W. Kockelmann, L.C. Chapon, P.G. Radaelli, Neutron texture analysis on GEM at ISIS, Phys. B Condens. Matter 385–386 (2006) 639–643.
[40] H.-R. Wenk, L. Lutterotti, S.C. Vogel, Rietveld texture analysis from TOF neutron diffraction data, Powder Diffr. 25 (2010) 283–296.
[41] J.A. Gruber, S.A. Brown, G.A. Lucadamo, Generalized Kearns texture factors and orientation texture measurement, J. Nucl. Mater. 408 (2011) 176–182.
[42] J.L.W. Warwick, J. Coakley, S.L. Raghunathan, R.J. Talling, D. Dye, Effect of texture on load partitioning in Ti-6Al-4V, Acta Mater. 60 (2012) 4117–4127.
[43] B. Romanowicz, H.-R. Wenk, Anisotropy in the deep earth, Phys. Earth Planet. In. 269 (2017) 58–90.
[44] P. Bate, P. Lundin, E. Lindh-Ulmgren, B. Hutchinson, Application of laser-ultrasonics to texture measurements in metal processing, Acta Mater. 123 (2017) 329–336.